SAND2017-5514C

Finite Element Analysis of Weld Residual Stresses in Austenitic Stainless Steel Canisters in Dry Storage of Spent Fuel

Xin Wu[1], Zhenzhen Yu[1*], Scott Gordon[1], David Olson[1], Stephen Liu[1], Charles Bryan[2], Eric Schindelholz[2], David Enos[2] and Zeev Shayer[1]

[1]*George S. Ansell Department of Metallurgical and Materials Engineering, Colorado School of Mines, Golden, CO 80401*

[2]*Sandia National Laboratories, Albuquerque, NM 87185*

**Corresponding Author, email: zyu@mines.edu*

Keywords: Multi-pass welding, Residual stress, Finite element analysis, Deep-hole drilling, Contour method

1. Introduction

Chloride-induced stress corrosion cracking (CISCC) in the weldments of spent fuel canisters is one of the primary safety concerns during the dry storage of used nuclear fuel at Independent Spent Fuel Storage Installations (ISFSI) in coastal areas [1]. For SCC to occur, three criteria must be met: an aggressive chemical environment, susceptible microstructure, and sufficient tensile stress. Field sampling analysis of surface deposits on in-service SNF storage canisters at three near-marine ISFSI sites in the United States have demonstrated the presence of chloride-rich salts on the canister surfaces [2-4]. As part of the canisters' surface cools sufficiently for the salts to deliquesce, chloride-rich aqueous brine layer could form locally on the surface, leading to potential failures by CISCC in regions with high tensile stress. On the other hand, for austenitic stainless steel spent nuclear fuel (SNF) interim canisters, the multi-pass welding procedures introduces high tensile residual stress and sensitization in the heat-affected zone (HAZ). Therefore, the potential for CISCC in the weldments of the stainless steel interim storage canisters has been identified as a high priority data gap.

To gain a fundamental understanding of the pitting and cracking behavior in the canisters and to accurately predict their long-term performance, the first step is to obtain the accurate residual stress distribution within the canisters, especially in the weldments. In the last decade, there have been several studies on the residual stress in the canister welds. For example, Kosaki et al. [5] reported that the experimentally measured weld residual stresses were close to the yield stress through thickness on a cylindrical canister of 1.3 m in diameter and with walls ~75 mm thick. The Nuclear Regulatory Commission (NRC) simulated the residual stresses for typical canister welds by employing a two-dimensional sequentially coupled thermal-structural finite element (FE) model [6], and predicted that tensile stresses of sufficient magnitude to initiate SCC are likely to present in the HAZ of both longitudinal and circumferential welds through the wall thickness of the canisters, allowing for crack propagation through the wall thickness over time. There is very limited literature on 3D simulation of the residual stress induced by multi-pass longitudinal and circumferential welds in the dry storage fuel canisters. In this study, a 3D FE model using ABAQUS software is built to simulate the residual stress contours in the 304 stainless steel canisters with the presence of both the longitudinal and circumferential multi-pass welds. Experimental measurements by deep-hole drilling (DHD) and contour methods provide valuable comparisons with the simulation results.

2. Computation Procedure

ABAQUS software was used to build the 3D model for longitudinal and circumferential double-V groove multi-pass welds in a full-diameter mockup canister, as shown in Fig. 1. The mockup consists of three cylindrical shells that are 1.22 m (48 inch) long and 1.71 m (67.2 inch) in diameter with a wall thickness of 15.9 mm (5/8 inch). Each shell was cold formed from a plate into a cylinder and then welded by the longitudinal multi-pass weld. The three cylinders were then welded together by two circumferential multi-pass welds. All of the welds were made by submerged-arc welding (SAW). The inner diameter was welded first, followed by the outer diameter. Detailed weld parameters can be found in reference [7]. The container was made by 304/304L stainless steel, and weld filler metal was 308L stainless steel.

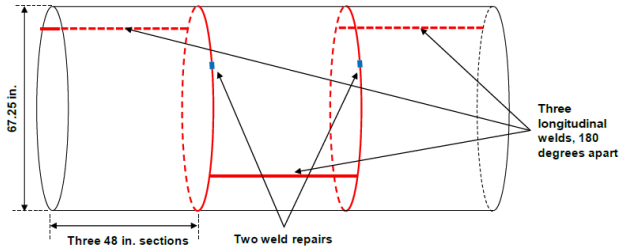

Fig. 1. Schematic representation of the full-scale mock storage container

The 3D FE model is shown in Fig. 2 with 52100 brick elements. Since the three longitudinal welds were made individually in experiment, and the spatial distance between the circumferential welds were relatively large, the interaction between the welds of the same type can be considered negligible. Therefore, only one longitudinal and circumferential weld was considered in this model. The FE model is further simplified to simulate only half of longitudinal and circumferential welds, respectively, which is sufficient to cover the steady state of the welding process, but the heat source still went through the whole length of the welds to make sure the elements experience the same thermal history as in the real case. In the model, the nonlinear transient heat conduction analysis was performed first to get the temperature distribution during each welding pass. Then, the temperature history result was employed as a thermal body load in the subsequent non-linear mechanical elastic-plastic calculation to obtain the residual stress distribution. The model change option was used to simulate the weld metal deposition, which means during the first weld pass, the other weld pass elements were killed. After the first weld was finished, the elements for the second pass were made active to simulate the weld metal deposition into the groove. Similarly, during the longitudinal welding passes, the circumferential weld elements were not activated.

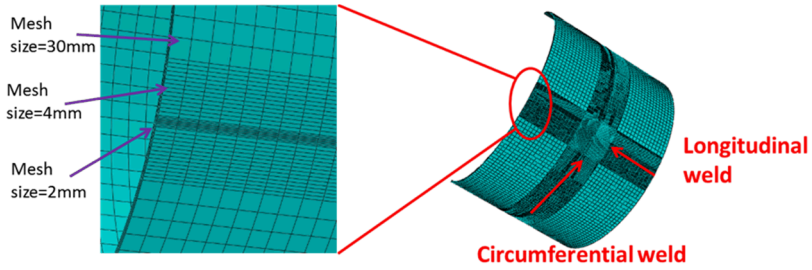

Fig. 2. 3D FE model of the longitudinal and circumferential welds in the canister mockup

As shown in Fig. 3, the multi-pass weld bead has sharp transition angles, which requires extremely fine meshes. More importantly, the cross section of longitudinal and circumferential welds needs compatible meshing. Due to such complications, the weld beads from experiment were divided into many small rectangle-shaped areas as in Fig.3. Then, the weld bead used in the finite element analysis (FEA) was assigned by combining the small areas to match the bead morphology as closely as possible, which avoided the elements with sharp angles and made the FEA converge more easily.

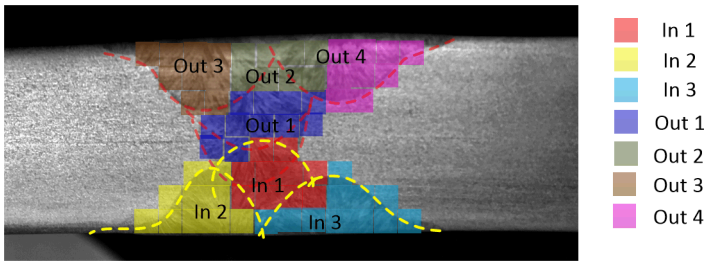

Fig. 3. Experimental bead morphology (dotted line) and corresponding computational bead morphology (colored regions)

The mockup base material is 304 stainless steel, and the material properties of 304 used in the simulation were taken from reference [8]. Because reference [8] doesn't include the hardening data, the temperature-dependent hardening property was from reference [9]. The material's solidus and liquidus temperatures were considered as 1400 and 1450 □, respectively. The latent heat of fusion was taken as 260 kJ/kg, to include the thermal effects due to solidification of the weld metal. The material properties were assumed to be the same for both base and weld metals.

Double-ellipsoidal heat source model developed by Goldak [10] was used to simulate the heat input of submerged-arc welding process. Figure 4 shows the heat flux distribution. The front and rear of the heat flux are descried by Eqs. (1) and (2), respectively:

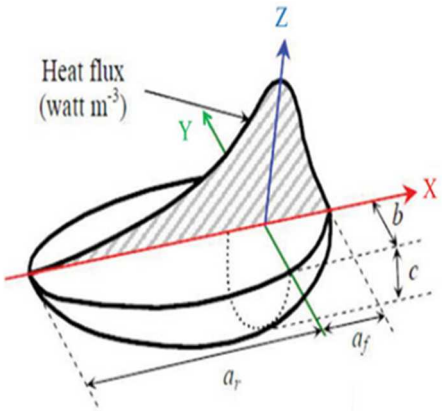

Fig. 4. Heat source model for the welding simulation.

$$q_r(x, y, z) = \frac{6\sqrt{3} f_r \eta Q}{a_r bc\pi\sqrt{\pi}} \exp\left(-\frac{3x^2}{a_r^2} - \frac{3y^2}{b^2} - \frac{3z^2}{c^2}\right) \quad (1)$$

$$q_f(x, y, z) = \frac{6\sqrt{3} f_f \eta Q}{a_f bc\pi\sqrt{\pi}} \exp\left(-\frac{3x^2}{a_f^2} - \frac{3y^2}{b^2} - \frac{3z^2}{c^2}\right) \quad (2)$$

where the front and rear quadrant fractions, f_f and fr, are set as 0.6, 1.4 respectively. The heat input Q=V*I*η, where voltage V=30V, current I=400A and heat source efficiency η=0.8. a_f, a_r, b, c are set to be 12, 24, 13, 13, respectively, to match the fusion boundary as observed in Fig. 2.

3. Results and Discussion

3.1 Residual Stress Contours

Fig. 5 summarizes the residual stress contours of the mockup after welded by seven longitudinal weld passes and eight circumferential weld passes. It is observed that the highest tensile stresses are always parallel to the welding direction. For instance, in the longitudinal welds, as shown in Fig. 5 (a), the axial stress is as high as 423.7 MPa in the weld center, which is much higher than the hoop stress. In comparison, a maximum residual stress of 366.1 MPa lies in in hoop direction in the circumferential welds. The influence of two intersecting multi-pass weldments on the residual stress distribution is clearly demonstrated in Fig.5 as well.

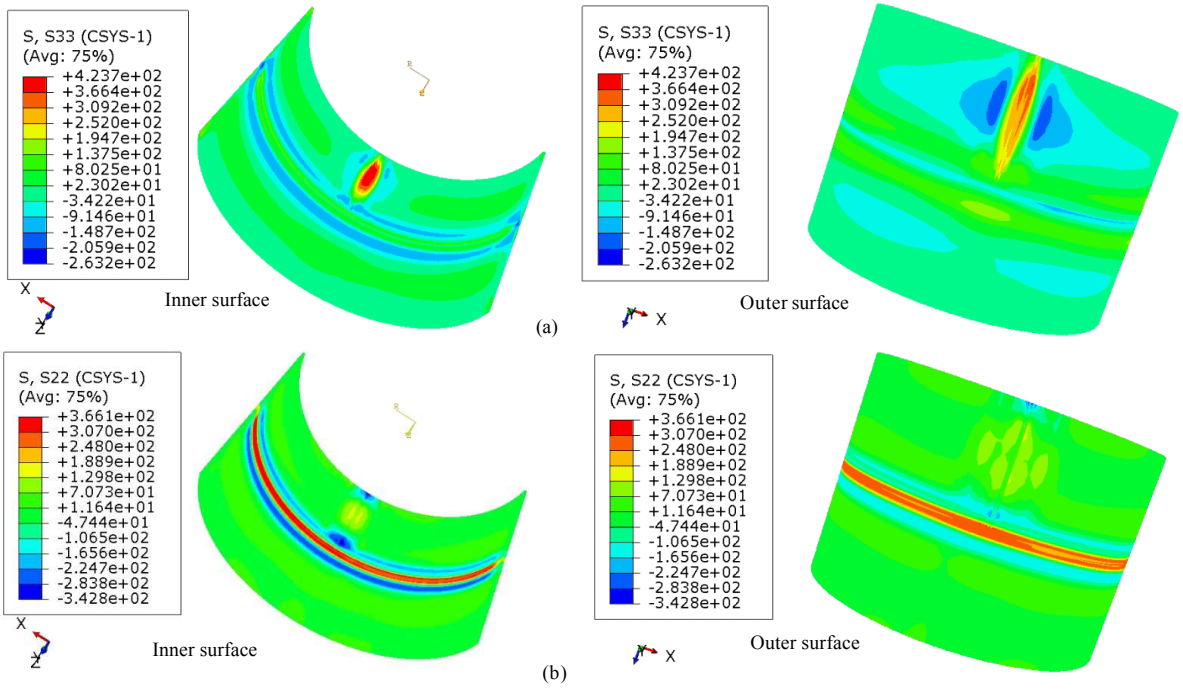

Fig. 5. Residual stress countours of (a) axial stress and (b) hoop stress on the inner and outer surfaces, respectively.

3.2 Comparison of FEA with Measurement Results

Fig. 6 compares the residual stress profiles as a function of depth in circumferential weld centerline and HAZ obtained from FEA and DHD measurements, which demonstrates good agreement. The lower residual stress near the inner and outer surfaces from DHD measurements than the simulation results may be caused by the cold forming or rolling process in the base metal prior to welding, which is not considered in the FE model. It is observed in Fig. 6 that the stress is strongly tensile through the entire thickness of the container wall in the hoop direction within the weld and HAZ. In the longitudinal welds (not shown here), high tensile axial stress is present through thickness in the weld and HAZ as well.

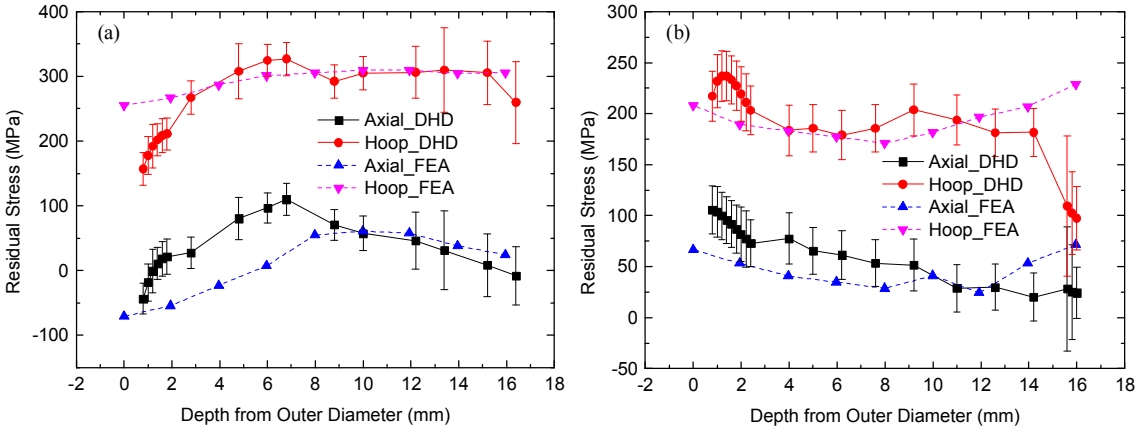

Fig. 6. Residual stresses profiles in (a) weld centerline and (b) HAZ of circumferential weld from FEA (dashed lines) and DHD measurements (solid lines). The data in HAZ was taken about 4 mm away from the weld toe.

The cross-section stress contour is extracted from FEA results, and compared with the results from contour method for both circumferential and longitudinal weld. Fig. 7 demonstrates the comparison of longitudinal weld. Good agreement is achieved between the FEA and contour measurement results. The residual stresses are strongly tensile through thickness near the longitudinal weld centerline. The simulation result predicts a slightly wider tensile residual stress regime than the contour method, especially on the inner and outer surfaces, which is in agreement with the experimentally observed fusion boundary morphology as illustrated in Fig. 3. Note that tensile stress is observed at the two ends of the welded plate in the contour method, as shown in in Fig. 7(a), which could be potentially introduced by cutting process.

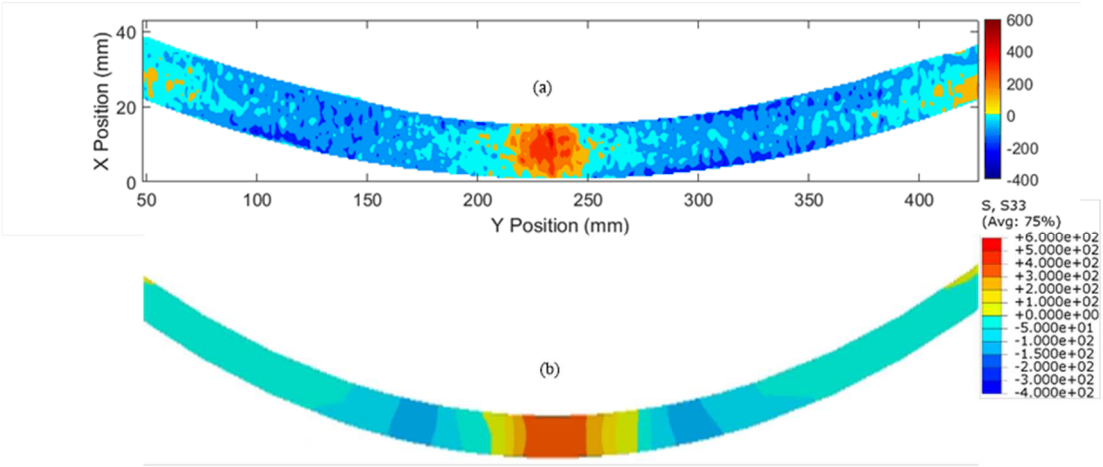

Fig. 7. Cross-section axial stress contour distribution for longitudinal weld from (a) contour method and (b) FEA

4. Conclusions

(1) A 3D sequentially coupled thermo-mechanical FE model was built to simulate the residual stresses induced by two intersecting longitudinal and circumferential multi-pass welds in austenitic stainless steel mockup canisters for dry storage of spent fuel. The welding parameters in the model followed the actual manufacturing procedures for the canister mockup. The predicted welding residual stress distribution agreed well with the experimental measurements.

(2) Based on the simulation and experimental measurement results, high through-thickness hoop stresses were found within the weld metal and HAZ in circumferential welds. In comparison, high through-thickness axial stresses were observed in the weld metal and HAZ in longitudinal welds.

(3) On the outer surface of the canister, where CISCC is likely to initiate, FE analysis predicted that the maximum residual stress in HAZ 4mm away from the weld toe was about 210 MPa (hoop) in circumferential weld and about 140 MPa (axial) in the longitudinal weld, respectively. In the weld centerline, the maximum residual stress on the outer surface was predicted to be about 250 MPa (hoop) and 300 MPa (axial) in circumferential and longitudinal welds, respectively.

Acknowledgements:
This work was supported by the DOE, Nuclear Engineering University Program (NEUP) under grand number DE-NE0008442 of Integrated Research Program (IRP), no. IRP-15-9318.

References:
[1] R.M. Kain, "Marine Atmospheric Stress Corrosion Cracking of Austenitic Stainless Steels", Materials Performance, 29 (12), 60 (1990).
[2] D.G. Enos, C.R. Bryan, and K. M. Norman, "Data Report on Corrosion Testing of Stainless Steel SNF Storage Canisters", FCRD-UFD-2013-000324. U.S. Department of Energy, Office of Used Nuclear Fuel Disposition, (2013).
[3] C.R. Bryan, and D.G. Enos, "Analysis of Dust Samples Collected from Spent Nuclear Fuel Interim Storage Containers at Hope Creek, Delaware, and Diablo Canyon, California", SAND2014-16383. Albuquerque, NM. Sandia National Laboratories, (2014).
[4] C.R. Bryan, and D.G. Enos "Analysis of Dust Samples Collected from an Unused Spent Nuclear Fuel Interim Storage Container at Hope Creek, Delaware", SAND2015-1746. Albuquerque, NM. Sandia National Laboratories, (2015).
[5] A. Kosaki, "Evaluation method of corrosion lifetime of conventional stainless steel canister under oceanic air environment", Nuclear Engineering and Design, 238 (5), 1233-1240 (2008).
[6] Nuclear Regulatory Commission (NRC), "Finite Element Analysis of Weld Residual Stresses in Austenitic Stainless Steel Dry Cask Storage System Canisters", NRC Technical Letter Report (ADAMS ML13330A512), 37, Washington, D.C. (2013).
[7] D.G. Enos, and C.R. Bryan, "Characterization of Canister Mockup Weld Residual Stresses", Sandia National Laboratories, FCRD-UFD-2016-000064, SAND2016-12375 R, (2016)
[8] D. Dean, and M. Hidekazu, "Numerical simulation of temperature field and residual stress in multi-pass welds in stainless steel pipe and comparison with experimental measurements", Computational Materials Science, 37, 269-277(2006).
[9] C. Liu, J. X. Zhang, C. B. Xue, "Numerical invetigation on residual stress distribution and evolution during multi-pass narrow gap welding of thick-walled stainless steel pipes", Fusion Engineering and Design, 86, 288-295 (2011).
[10] J. Goldak, A. Chakravarti, M. Bibby, "A new finite element model for welding heat sources", Metall Trans B 15(2), 299–305 (1984).